Anisotropic excitonic magnetism from discrete C_4 symmetry in CeRhIn$_5$

D. J. Brener [1] I. Rodriguez Mallo [2] H. Lane,[3] J. A. Rodriguez-Rivera [4,5] K. Schmalzl [6] M. Songvilay,[7]
K. Guratinder,[2] C. Petrovic,[8] and C. Stock [2]

[1]*The Higgs Centre for Theoretical Physics, University of Edinburgh, Edinburgh EH9 3JZ, United Kingdom*
[2]*School of Physics and Astronomy, University of Edinburgh, Edinburgh EH9 3JZ, United Kingdom*
[3]*School of Physics and Astronomy, University of St. Andrews, North Haugh, St. Andrews, Fife, KY16 9SS, United Kingdom*
[4]*NIST Center for Neutron Research, National Institute of Standards and Technology, 100 Bureau Dr., Gaithersburg, Maryland 20899, USA*
[5]*Department of Materials Science, University of Maryland, College Park, Maryland 20742, USA*
[6]*Forschungszentrum Juelich GmbH, Juelich Centre for Neutron Science at ILL, 71 avenue des Martyrs, 38000 Grenoble, France*
[7]*Université Grenoble Alpes, CNRS, Institut Néel, 38042 Grenoble, France*
[8]*Department of Physics, Brookhaven National Laboratory, Upton, New York, 11973, USA*

Anisotropy in strongly correlated materials is a central parameter in determining the electronic ground state and is tuned through the local crystalline electric field. This is notably the case in the CeCo$_x$Rh$_{1-x}$In$_5$ system where the ground-state wave function can provide the basis for antiferromagnetism and/or unconventional superconductivity. We develop a methodology to understand the local magnetic anisotropy and experimentally investigate with neutron spectroscopy applied to antiferromagnetic ($T_N = 3.8$ K) CeRhIn$_5$, which is isostructural to d-wave superconducting ($T_c = 2.3$ K) CeCoIn$_5$. Through diagonalizing the local crystal field Hamiltonian with discrete tetragonal C_4 point group symmetry and coupling these states with the random phase approximation, we find two distinct modes polarized along the crystallographic c and $a - b$ planes, agreeing with experiment. The anisotropy and bandwidth, underlying the energy scale of these modes, are tuneable with a magnetic field which we use experimentally to separate in energy single and multiparticle excitations thereby demonstrating the instability of excitations polarized within the crystallographic $a - b$ plane in CeRhIn$_5$. We compare this approach to a $S_{\text{eff}} = \frac{1}{2}$ parametrizations and argue for the need to extend conventional SU(2) theories of magnetic excitations to utilize the multilevel nature of the underlying crystal-field basis states constrained by the local point-group C_4 symmetry.

I. INTRODUCTION

Unconventional superconductivity is often found to coexist or be coupled with localized magnetic moments [1–3]. Noteworthy examples include the cuprate superconductors [4–6], iron based pnictide and chalcogenides [7,8], and nickel-based materials [9–11]. While cuprate and iron based compounds display large superconducting transition temperatures making them potentially useful for applications, the underlying energy scales in these compounds are large which makes them challenging to experimentally study. The strongly correlated and cooperative phenomena in these materials is fundamentally defined by single-ion energetics which fixes the ground state wave function. With the crystalline electric field defining the ground state magnetism in these materials set by $10Dq \sim 1$ eV [12–15], multiple experimental techniques are required to study magnetic and electronics properties of these compounds spanning a large energy scale.

Heavy fermion materials based on $4f$ elements, while displaying considerably lower superconducting transition temperatures, have much smaller crystalline electric field energetics and are therefore arguably more amenable for laboratory experiments. Illustrating this is CeCoIn$_5$ with a superconducting transition temperature of $T_c = 2.3$ K [16], yet displaying an unconventional d-wave order parameter [17,18] analogous to that observed in cuprate superconductors at considerably higher temperatures. $4f$ compounds therefore represent important case studies for competing magnetic and electronic phases. A unique aspect of magnetic $4f$ ions over $3d$ transition metal ions is the anisotropic crystalline electric field environment with an energy scale that is comparable to the magnetic exchange that couples magnetic ions. We investigate in this paper the consequences of this and also the crystalline anisotropy on the magnetic excitations. We focus on the Néel ordered phase in CeRhIn$_5$ which is a precursor and arguably parent to unconventional superconductivity in the CeXIn$_5$ series of compounds [19,20].

The heavy fermion CeXIn$_5$ series of materials display an interplay between various phases including density waves, helical and collinear magnetism, and d-wave superconductivity. Neutron spectroscopic studies of CeCoIn$_5$ report a magnetic resonance peak [21] tied with the formation of d-wave

superconductivity, illustrating an underlying coupling between magnetism and superconductivity. We note that similar spin resonances have been reported in multiple heavy fermion compounds which are both magnetic and unconventional superconductors [22,23]. This resonance peak in $CeCoIn_5$ is highly anisotropic [24] being polarized along the crystallographic c axis and is energetically doubly degenerate and can be split with an applied magnetic field [25–27]. While much attention has been given to $CeCoIn_5$ with its large (for heavy fermions) superconducting transition temperature, $CeRhIn_5$ has also been reported to be a superconductor with a much lower transition temperature of $T_c \sim 100$ mK at ambient pressures [28–30]. At higher temperatures of $T_N = 3.8$ K, $CeRhIn_5$ enters a helical magnetic phase. Superconductivity is enhanced with the application of pressure which also suppresses helical antiferromagnetism [31]. The goal of this paper is to understand the dynamics and magnetic ground state of the parent antiferromagnetic phase with the objective of relating it to the magnetic properties of its superconducting counterparts and in particular superconducting and non-magnetic $CeCoIn_5$. To accomplish this we discuss and theoretically analyze the magnetic dynamics of $CeRhIn_5$ as a function of applied magnetic field.

The magnetic field dependent phase diagram of $CeRhIn_5$ is illustrated in Fig. 1 as mapped out using neutron diffraction in Ref. [32] and displays three distinct phases. For low temperatures and small magnetic fields ("Phase I") $CeRhIn_5$ magnetism is defined by a helical phase along the crystallographic c axis with the periodicity defined by the wave vector $\vec{Q}_0 = (\frac{1}{2}, \frac{1}{2}, 0.297)$. Given that it is difficult to distinguish between a spin-density wave (where the magnitude of the magnetic moments modulate) and a helical magnetic phase (where the magnitude is fixed but direction rotates) on a Bravais lattice, polarized neutrons are required. This has been confirmed in Ref. [33] and illustrated in Fig. 1(b) with the helical nature evident from a projection along the crystallographic c axis. A transitional phase (identified as "Phase II") exists at intermediate fields and temperatures and is defined by an incommensurate wave vector of $\vec{Q}_0 = (\frac{1}{2}, \frac{1}{2}, 0.298)$ with a potentially elliptical structure [32]. This intermediate phase will not be discussed in this paper as we do not observe a clear signature of it in the excitations. A high-field and low temperature phase ("Phase III") is illustrated in Fig. 1(c) and consists of a commensurate block magnetic order defined by the wave vector $\vec{Q}_0 = (\frac{1}{2}, \frac{1}{2}, 0.25)$. We will focus our discussion below on the magnetic dynamics in the low temperature Phases I and III. The magnetic field thus provides a means to tune the magnetic structure from a helical incommensurate to a commensurate collinear phase.

In this paper we analyze the magnetic excitations of $CeRhIn_5$ in the antiferromagnetic phase which is parent to unconventional superconductivity. We describe the single magnetic particle excitations using an "excitonic" model with coupled basis states defined by the single-ion crystal field Hamiltonian which incorporates magnetic anisotropy. This results in two distinct modes with polarization defined by the crystalline electric field, previously reported with neutron spectroscopy. We apply a magnetic field to identify strong multiparticle excitations and discuss possible origins of these excitations.
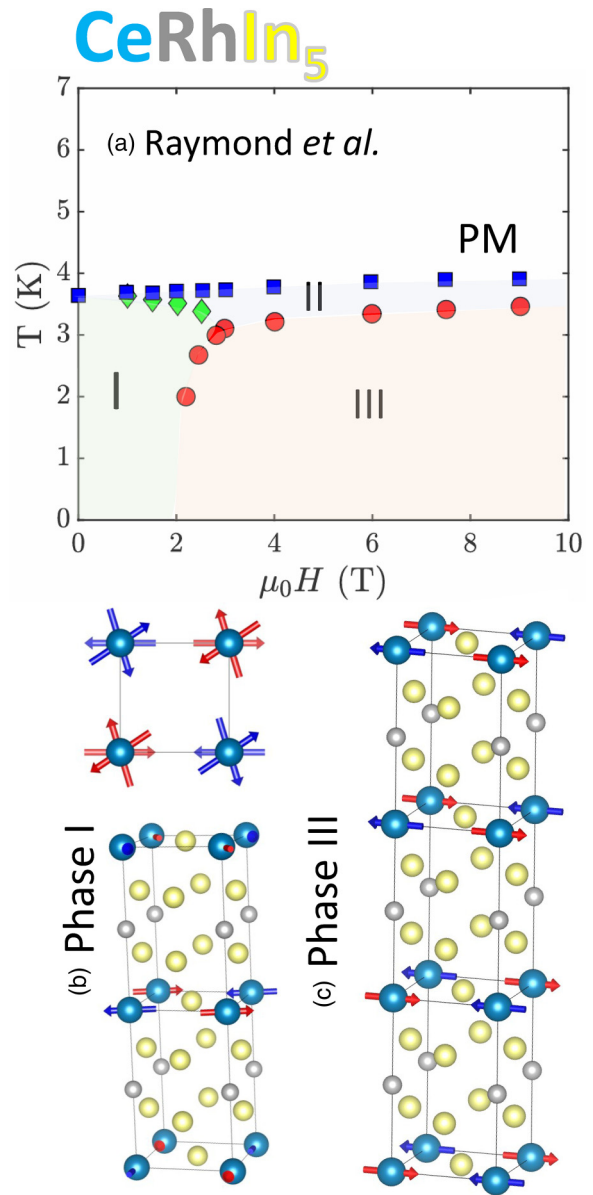

FIG. 1. The low temperature magnetic phases of $CeRhIn_5$. (a) The magnetic field-temperature phase diagram measured with neutron diffraction in Ref. [32]. (b) The zero field helical magnetic structure (Phase-I) defined by a propagation wave vector $\vec{Q}_0 = (\frac{1}{2}, \frac{1}{2}, 0.297)$. (c) The high magnetic field and low temperature magnetic structure (Phase-III) defined by the wave vector $\vec{Q}_0 = (\frac{1}{2}, \frac{1}{2}, \frac{1}{4})$.

II. EXPERIMENT

To probe the low-energy magnetic excitations we have applied neutron spectroscopy, which is directly sensitive to dipole allowed fluctuations. In this paper we present data on the magnetic field dependence of the magnetic excitations in $CeRhIn_5$. The sample is the same as used in Ref. [33]. The experiments were performed on the MACS triple-axis spectrometer at NIST (Gaithersburg, USA) [34]. Given the need to sample a large region of momentum space, the multidetector arrangement and large flux on the sample was advantageous. Cooled filters of beryllium were used after the sample with the final energy fixed by a double bounce PG(002) analyzer with
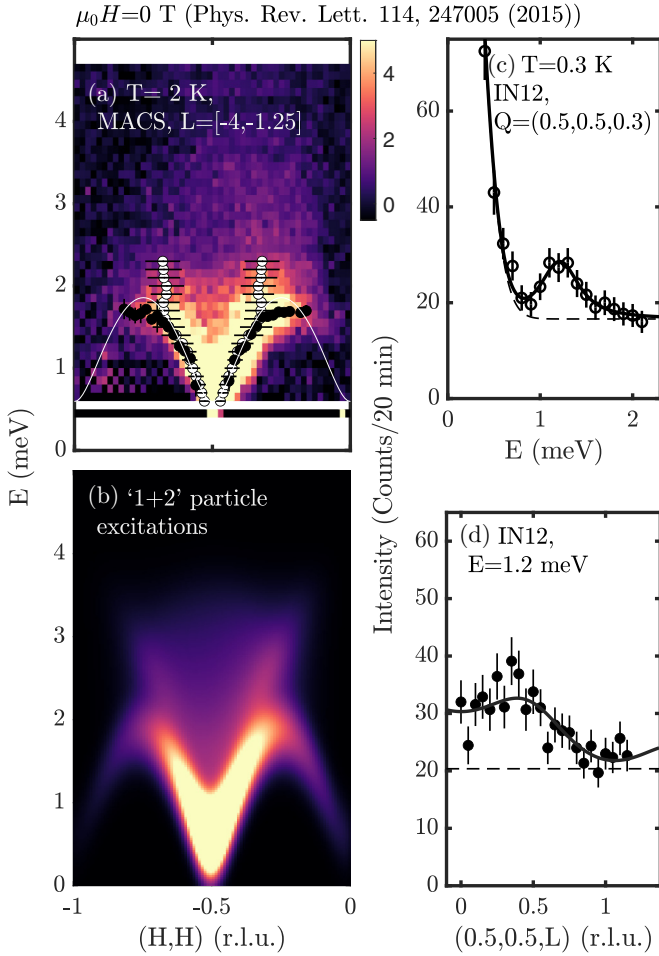
FIG. 2. A summary of the zero field magnetic fluctuations in $CeRhIn_5$ below T_N previously reported based on neutron spectroscopy. (a) Neutron spectroscopy measurements on MACS compared against a (b) heuristic multimagnon calculation. A second gapped mode is found in (c) using IN12 which corresponds to fluctuations polarized along the crystallographic c axis as confirmed from a scan of the intensity along [001] shown in (d).

$E_f = 5.1$ meV and E_i defined by a double focused PG(002) monochromator. The sample was mounted in a 11 T vertical magnetic field such that reflections of the form (HHL) lay within the horizontal scattering plane and cooled to temperatures as low as 0.5 K, well within the antiferromagnetically ordered phase of $CeRhIn_5$ ($T_N = 3.8$ K).

III. RESULTS

A. Zero-field results summary

We first review the magnetic excitations at zero applied field and summarized based on our previous results [33] in Fig. 2. Figure 2(a) illustrates the magnetic excitations measured on the MACS spectrometer (NIST). These excitations emanate from the commensurate $(\frac{1}{2}, \frac{1}{2})$ position with no observable momentum dispersion along L. The solid black points are the peak positions extracted from one-dimensional constant momentum cuts through the data and the white open circles are from analogous constant energy cuts. Along with a

band of magnetic excitations, which is defined by the instrument resolution in momentum and energy (hence well defined and underdamped), a momentum and broadened continuum of excitations is observable up to at least 4 meV. This is parameterized in terms of multiparticle (or "2 magnon") in Fig. 2(b) as discussed in Ref. [33].

The experimental data in Fig. 2(a) is integrated over a wide range of momentum transfers along L owing to the two-dimensional nature of the magnetic fluctuations. Because of selection rules of magnetic neutron scattering which impose that the cross section is sensitive to magnetic moments *perpendicular* to the momentum transfer, Fig. 2(a) is primarily sensitive to fluctuations within the crystallographic $a - b$ plane. To probe magnetic fluctuations polarized along the crystallographic c-axis, Ref. [33] used IN12 (ILL) to study magnetic fluctuations at small L momentum transfers and hence more sensitive to fluctuations polarized perpendicular to the crystallographic $a - b$ plane. The results are summarized through a constant momentum scan in Fig. 2(c) and a constant energy scan in Fig. 2(d) illustrating the decay of intensity with increasing momentum transfer along L indicative that these excitations correspond to fluctuations polarized along the crystallographic c axis. This is further confirmed by results presented in Ref. [35] which present time-of-flight data illustrating the presence of at least two distinct underdamped magnetic modes.

The zero field neutron response consists of both single-particle (underdamped and well defined in momentum and energy) and multiparticle (momentum and energy broadened) components. The single-particle component consists of two bands with a low-energy band dispersing from the commensurate $\vec{Q} = (\frac{1}{2}, \frac{1}{2})$. These excitations are polarized within the crystallographic $a - b$ plane. The higher energy mode illustrated in Fig. 2(c) corresponds to fluctuations along the crystallographic c axis.

B. Results in applied magnetic field

We now discuss the magnetic excitation spectrum at low temperatures in the antiferromagnetic phase with an applied field along the [1$\bar{1}$0] direction with the results summarized in Fig. 3. For a small magnetic field of $\mu_0 H = 1.5$ T [Fig. 3(a)], where the static magnetism remains within the helical "Phase I" (Fig. 1), little qualitative change is observed from zero field results (Fig. 2). On entering the collinear "Phase III" the single particle band becomes clearly gapped at the magnetic zone center, indicative of an anisotropy, as shown in momentum-energy maps at $\mu_0 H = 7.25$ and 9 T] Figs. 3(b) and 3(c)]. The bandwidth of the lower energy single band also decreases and this is evidenced on comparison of Fig. 3(b) ($\mu_0 H = 7.25$ T) and Fig. 3(c) ($\mu_0 H = 9$ T). This indicates that the exchange interaction between Ce^{3+} ions is weakened on application of an in-plane magnetic field. These results are generally consistent with the increase in the anisotropy gap and also the decrease in exchange parameters noted in Ref. [36] for $CeRhIn_5$ using chopper spectrometers focusing on in-plane excitations at small values of L.

On increasing the magnetic field, the energy and momentum broadened multiparticle excitations observed at zero field in Fig. 1 sharpen and become more well defined in
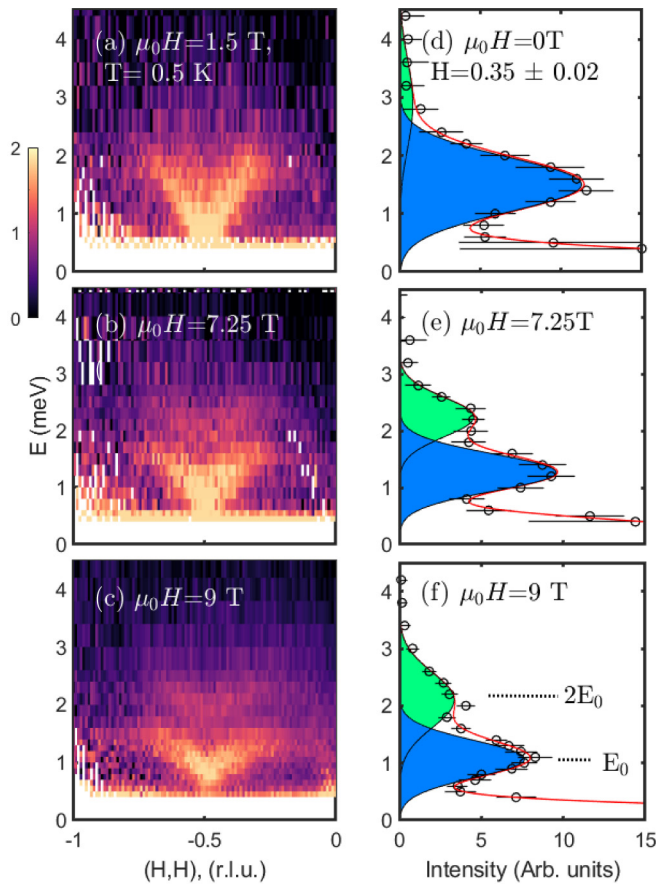
FIG. 3. Evolution of the magnetic field spectrum in a vertical applied magnetic field along the $[1\bar{1}0]$ direction. (a)–(c) display momentum-energy maps at $\mu_0 H = 1.5$, 7.25, and 9 T. (d)–(f) display cuts at each field at H = 0.35 ± 0.02 rlu.

momentum and energy. This is particularly evident in the momentum-energy map in Fig. 3(c) at $\mu_0 H = 9$ T and the one-dimensional cut at H=0.35 ± 0.02 r.l.u. in Fig. 3(f). There are two modes in the neutron spectra seen at $\mu_0 H = 9$ T with the upper mode being a factor of 2 at higher energies than the lower mode. This is also evident at $\mu_0 H = 7.25$ T displayed in Fig. 3(b) and in the one-dimensional cut in Fig. 3(e). This second mode can be understood in terms of a multiparticle process based on the lower mode. With the application of a magnetic field, the energetic gap at the magnetic zone center increases along with the bandwidth of the mode decreasing. This sharpening in energy of the lower single particle branch narrows the allowed multiple particle phase space permitted through exciting two single magnons. In the limit where there is nearly no momentum dispersion, the single and multiparticle processes would consist of two flat in momentum excitations separated by a factor of 2. The application of a magnetic field in CeRhIn$_5$ clearly shows the existence of a multiparticle process at higher energies with energy and bandwidth tunable using an applied magnetic field. This demonstrates that the low-energy mode discussed above in the context of the $\mu_0 H = 0$ T data, which is polarized within the crystallographic $a - b$ plane, is unstable to multiparticle processes.

IV. THEORY

In this section we aim to understand the excitations presented above. We first discuss various approaches to modeling the magnetic fluctuations and then apply these to the case of CeRhIn$_5$ in a magnetic field. Notably, we compare and contrast the "effective spin" and "excitonic" approaches to this problem that are discussed in the context of the underlying symmetry groups that are important for the magnetic excitations. SU(2) provides an interesting example of this as the SU(2) group covers O(3) which has a continuous rotational symmetry requiring a gapless Goldstone mode in the magnetic excitation spectrum for a Hamiltonian with SU(2) symmetry. This is an example where the symmetry group has consequences on the predicted magnetic excitations. We use Co^{2+} and CoO as an illustrative example to motivate the distinction and need for various approaches for magnetic excitations [14,37,38].

Effective "spin" (j_{eff}) spin-wave approach. Magnetic excitations are typically dealt with in the field of scattering in terms of searching out solutions of the Landau-Lifshitz equation for an "effective" spin of fixed length under the constraints of a magnetic Hamiltonian which accounts for interactions between spatially separated magnetic ions. The Hamiltonian is built up from Heisenberg interactions between these effective spins. We note that the resulting Hamiltonian may not have the same symmetry as these spins with weak anisotropic terms introduced for parametrization purposes.

This approach can be applied to transition metal compounds containing Co^{2+} with small exchange coupling and hence small molecular field environments. This has been shown by us in our study of CoO [37] where the single-ion Hamiltonian, incorporating crystalline electric field and spin-orbit terms, can be rotated to form a block diagonal matrix. In terms of group theory, this is identical to formulating the irreducible representations. The ground state Kramers doublet of Co^{2+} in an octahedral crystalline electric field is isomorphic with SU(2) and the underlying Lie algebra generators are proportional to the 2×2 Pauli matrices [38].

The entire single-ion energy spectrum, from a Hamiltonian consisting of crystalline electric and spin-orbit coupling terms in an isolated Co^{2+} ion, results in three energy multiplets with each having a total effective angular momentum (which also defines the degeneracy) of $j_{eff} = \frac{1}{2}$, $\frac{3}{2}$, and $\frac{5}{2}$. We note that the constant of proportionality, or the projection factors, that allow mapping onto effective angular momentum operators, are isotropic scalars. For cases where the ground state $j_{eff} = \frac{1}{2}$ manifold is energetically well separated from higher energy j_{eff} levels an effective Hamiltonian can be constructed for the excitations within only the ground state Kramers doublet based on interacting $S = \frac{1}{2}$ operators. This in turn facilitates excitations to be calculated using time evolution defined by the Landau-Lifshitz equation ($\frac{d}{dt}\langle S \rangle = h_{MF} \times \langle S \rangle$).

Interacting multilevel approach. However, in the case of CoO where, and unusually in transition metal ions, the exchange interaction, spin-orbit coupling, and crystalline electric field distortion parameters are all comparable and the three j_{eff} eigenstates of the single-ion Hamiltonian are strongly mixed. This invalidates the effective spin $S_{eff} = \frac{1}{2}$ approximation discussed above and requires the multilevel

single-ion eigenstates to be coupled and accounted for rather than parametrization in the magnetic Hamiltonian.

We have followed the study of interactions between quasiparticles in electronic models where the single-particle Greens function is fundamental for accounting for interactions. In the case of insulating magnetic systems, and the approach we take here, this single-particle Green's function is constructed based on the single-ion Hamiltonian to reflect the underlying crystalline electric field. Such a Hamiltonian naturally accounts for the lattice space group symmetry and indeed the eigenvectors form a representation of the space group [39]. Instead of the conventional approach utilizing pseudoboson operators in SU(2) as a starting point for perturbation, this approach accounts for the N-multilevel nature and is akin to SU(N) theory developed for magnetic excitations [40–43] which brings in other members of the Lie algebra beyond the dipole operators.

Case of CeRhIn$_5$. For the rare-earth system of interest here, the magnetic ion is the $4f$ element Ce^{3+}. Given that spin-orbit coupling is considered as the dominant energy scale in the magnetic Hamiltonian in $4f$ elements, the observable operators which commutes with the Hamiltonian, and from which the eigenvalues define the good quantum numbers, are the components of the total angular momentum operator $\vec{J} = \vec{L} + \vec{S}$. In the case of Ce^{3+}, the total angular momentum corresponds to $j = \frac{5}{2}$. The six basis states (that are eigenvectors of the observable J_z), in the presence of crystalline electric field, break up into doubly degenerate levels. Since the crystalline electric field is symmetric under time reversal symmetry, Kramers' theorem [44] applies and the doublet degeneracy cannot be broken unless a time reversal symmetry breaking field (e.g., Zeeman magnetic or molecular field) is introduced.

A. Effective-spin model

We first review the conventional effective $S = \frac{1}{2}$ model to parametrize the magnetic excitations [44]. In this case, we assume that the ground state Kramers doublet is separated in energy from the first excited Kramers doublet by an energy much greater than the temperatures of the experiment. In such a case, the ground state two-level single-ion doublet can be mapped to a pseudospin $S = \frac{1}{2}$ particle in a magnetic field [45]. This approach starts with assuming SU(2) symmetry and parameterizes the Hamiltonian with anisotropy as

$$\mathcal{H} = J \sum_{ij} \left(S_i^x S_j^x + S_i^y S_j^y + \Delta S_i^z S_j^z \right),$$

where J is the magnetic exchange coupling between neighboring spins defined by the indices i, j. The parameter Δ defines a comparatively weak anisotropy along the crystallographic c axis. We note that while the starting operators form an algebra of SU(2), the Hamiltonian does not have SU(2) symmetry and this can be seen by the fact that observable operators $S_{x,y}$ do not commute with the anisotropy term set by the parameter Δ.

The neutron response for magnetic moments of fixed spin S on a two-dimensional lattice is well established [46,47]. The magnon dispersion takes the form

$$E(\mathbf{q}) = 4JS\sqrt{(1+\Delta)^2 - \gamma^2(\mathbf{q})},$$

where $\gamma(\mathbf{q}) = \cos[\pi(H+K)]\sin[\pi(-K+H)]$. This parametrization approach to the data in terms of an exchange coupling between nearest-neighboring spins was applied in both Refs. [33] and [35] to describe the low-energy single-particle excitations in CeRhIn$_5$. Reference [35] included several different exchange constants to account for both the ordering wave vector and multiple modes. Reference [33] parameterized the lowest energy excitation, corresponding to in-plane fluctuations above, by a single exchange parameter. While such an approach has real utility for efficiently computing estimates of nearest-neighbor in-plane exchanges, it does not capture the anisotropy of the magnetic excitations without an additional effective parametrization of the magnetic Hamiltonian.

B. Excitonic models and Kramers doublet magnetism

Having discussed the effective $S = \frac{1}{2}$ model which is anchored in SU(2) in the previous section, we now apply an excitonic approach including the multilevel nature of the isolated Ce^{3+} ion in a crystalline electric field. This approach differs from the effective $S = \frac{1}{2}$ model defined above. Instead of starting by considering isotropic $S = \frac{1}{2}$ SU(2) operators corresponding to a two-level system approximating the ground state Kramers doublet of Ce^{3+}, we consider the full $j = \frac{5}{2}$ multiplet with the energetically Kramers degenerate states split by a local crystalline electric field and nearby molecular fields from ordered magnetic moments. These eigenstates of the crystalline electric field Hamiltonian are then coupled using a mean-field random phase approximation (RPA). We note that this approach involves a starting basis defined by the crystalline electric field, which is six-dimensional (corresponding to $|j \equiv \frac{5}{2}, m\rangle$ eigenstates of the J_z observable in the fundamental representation). These states are then used as a basis to diagonalize the electrostatic Hamiltonian built from Stevens' operator equivalents. The resulting single-ion eigenstates are then coupled via dipole operators of angular momentum and we calculate the neutron cross section by applying the Green's function formalism for magnetic dynamics. The approach treats the importance of anisotropy [48] in the heavy fermions on an equal scale with applied field and interactions.

Note that this differs from that of effective $S = \frac{1}{2}$ theories crucially in terms of symmetry properties. The anisotropy defined by the local crystal electrostatic field is built into the starting multiple single-ion eigenstates. This is in contrast to parametrizing the Hamiltonian in terms of the anisotropic terms deviating from the symmetric Heisenberg interaction in the effective $S = \frac{1}{2}$ model. We note that our previous theoretical work on Ca$_2$RuO$_4$ [49] illustrated the utility of this multilevel approach allowing model terms to be readily mapped to real physical quantities, and also minimizing additional parameters terms in the magnetic Hamiltonian.

1. Total magnetic Hamiltonian

In the following section we pursue this method by first discussing the single-ion Hamiltonian defined by the local crystalline electric field and then the coupling of the eigenstates of the Hamiltonian using the RPA [50]. This procedure requires the total Hamiltonian to be divided into two parts

TABLE I. Stevens operators relevant for CeRhIn$_5$ from Ref. [52].

$\mathcal{O}_2^0$	$3J_z^2 - J^2$
$\mathcal{O}_4^0$	$35J_z^4 - 30J^2J_z^2 + 25J_z^2 - 6J^2 + 3(J^2)^2$
$\mathcal{O}_4^4$	$\frac{1}{2}(J_+^4 + J_-^4)$

with one describing the single-ion response and the second corresponding to interactions between neighboring magnetic moments. We define this overall Hamiltonian as

$$\mathcal{H}_{\text{tot}} = \mathcal{H}_{SI} + \mathcal{H}_{\text{inter}}. \tag{1}$$

We first discuss the single-ion Hamiltonian $\mathcal{H}_{SI}$ and then interactions through $\mathcal{H}_{\text{inter}}$ below.

2. Single ion - Local electrostatic and molecular fields

Based upon symmetry considerations [51] of the point group of the magnetic ion in CeRhIn$_5$ (Fig. 1), the electrostatic Hamiltonian for isolated Ce^{3+}, $j = 5/2$ in a tetragonal crystal field is given by the following equation in terms of Stevens' operators ($\mathcal{O}_2^0$, $\mathcal{O}_4^0$, and $\mathcal{O}_4^4$) and scalar parameters (B_2^0, B_4^0, and B_4^4):

$$\mathcal{H}_{CEF} = B_2^0\mathcal{O}_2^0 + B_4^0\mathcal{O}_4^0 + B_4^4\mathcal{O}_4^4. \tag{2}$$

The Stevens' operators ($\mathcal{O}_2^0$, $\mathcal{O}_4^0$, and $\mathcal{O}_4^4$) are defined [52] (reproduced in Table I) in terms of the angular momentum operators $J_{x,y,z}$ ($J_\pm \equiv J_x \pm iJ_y$) and J^2 (which is proportional to the identity) and the variables (B_2^0, B_4^0, and B_4^4) which are real constants that act as parameters for the local crystalline electric field. We note that the crystal field parameters are the same for the C$_4$, S$_4$, and C$_{4v}$ point group symmetries [51]. For the purposes of the discussion here we will discuss the arguably simplest case of the C$_4$ point group which consists of four symmetry operations including the identity operator. The three Stevens' parameters can be fit from neutron data and also calculated using, for example, point-charge calculations based on Coulomb electrostatic fields.

The local crystalline electric field in CeXIn$_5$ has been discussed extensively in previously published papers. We will use the crystal field Stevens' parameters reported in Refs. [53,54] for CeRhIn$_5$. We note that both Ref. [53] and Ref. [54] give consistent answers for the ground state wave functions in CeRhIn$_5$ and therefore we have used the average value in our calculations. These are summarized in Table II. Real space plots of the wave functions and a discussion of hybridization is given in Ref. [55].

Diagonalizing the six-dimensional $\mathcal{H}_{CEF}$ in Eq. (2) gives three sets of doublets for a total of six eigenstates for the crystalline electric field Hamiltonian. The effect of each of

TABLE II. Stevens coefficients taken from Refs. [53] and [54]. Averages used in our calculations are given in the last column.

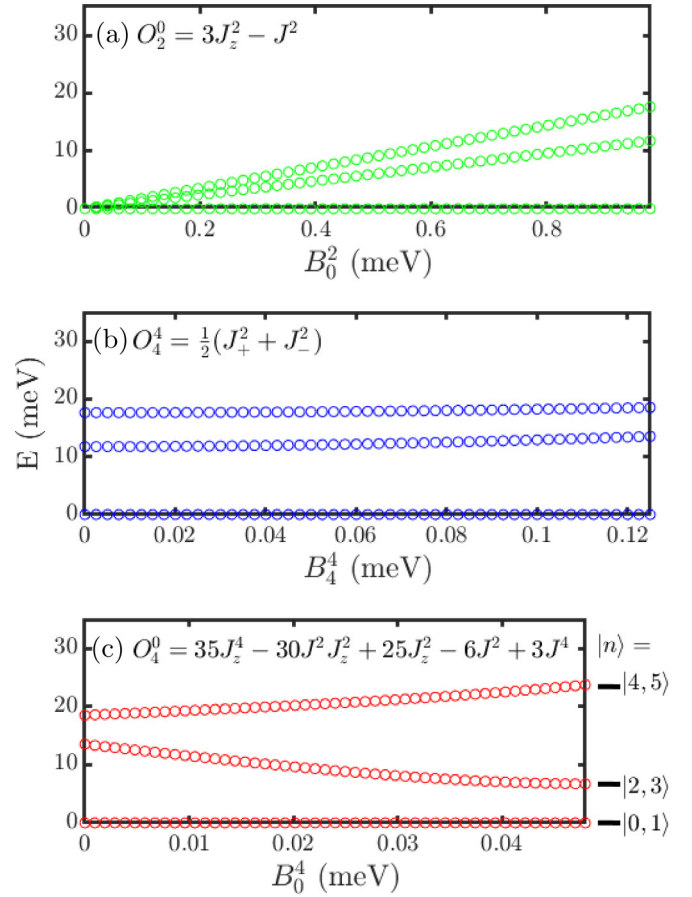| B_l^m	Ref. [53]	Ref. [54]	Average
B_2^0	−1.03 meV	−0.928 meV	≡ −0.98 meV
B_4^0	0.044 meV	0.052 meV	≡ 0.048 meV
B_4^4	0.122 meV	0.128 meV	≡ 0.125 meV

FIG. 4. The energy eigenvalues of the electrostatic contribution to the single-ion Hamiltonian discussed in the text. In terms of Stevens' operators, the contributions from (a) O_2^0, (b) O_4^4, (c) O_4^0 are illustrated with the final set of three Kramers doublets shown.

the Stevens' operators in Eq. (2) is illustrated in Fig. 4 with the final energy eigenvalues shown in Fig. 4(c). As required by Kramers' theorem, these doublets cannot be split by a time reversal symmetry preserving crystalline electric field, but require a time reversal breaking field to break their doublet degeneracy. Such a field is present in the magnetically ordered phase at low temperatures where neighboring Ce^{3+} magnetic moments impose a molecular field on a given Ce^{3+} site by

$$\mathcal{H}_{MF} = h_{MF}J_z \tag{3}$$

where the scalar h_{MF} is discussed below when we describe the interaction term of the magnetic Hamiltonian. We discuss the effect of an applied magnetic field to the sample below in the context of this term in the single-ion Hamiltonian.

The total single-ion Hamiltonian in the low temperature phase is the sum of the crystal field and molecular field terms

$$\mathcal{H}_{SI} = \mathcal{H}_{CEF} + \mathcal{H}_{MF}, \tag{4}$$

where diagonalizing ($\mathcal{H}_{SI}|n\rangle = \omega_n|n\rangle$) gives the energy eigenvalue (ω_n) and eigenstates ($|n\rangle$) which we couple below.

3. Interion Hamiltonian-Isotropic Heisenberg exchange

Having presented the single-ion Hamiltonian that defines the multilevel basis states we wish to couple, in this section we

discuss the interion coupling of these states. To describe the interion coupling, we choose to take the simplest approach with the coupling to be bilinear in the angular momentum operators defined by

$$\mathcal{H}_{\text{inter}} = \frac{\mathcal{J}}{2} \sum_{i,j} \vec{J}_i \cdot \vec{J}_j, \tag{5}$$

where we take for simplicity $\mathcal{J}$ as a symmetric scalar which is analogous to the Heisenberg exchange discussed above in the context of the $S_{\text{eff}} = \frac{1}{2}$ analysis. We note that this approach naively assumes the exchange coupling between Kramers' doublets on differing sites is the same. The angular momentum observables are defined by $\vec{J}_i$ with $J^2 = J_x^2 + J_y^2 + J_z^2$ and $J^2|j, m\rangle = j(j+1)|j, m\rangle$ with $j = \frac{5}{2}$ and $J_z|j, m\rangle = m|j, m\rangle$.

While this approach works with a six-dimensional basis compared to a two-dimensional $S_{\text{eff}} = \frac{1}{2}$ parametrization discussed before, the anisotropy from the local crystalline electric field environment is directly incorporated into this new multilevel basis. Therefore, anisotropy terms are not used in the interacting Hamiltonian but is rather built into the starting basis derived from the crystal field Hamiltonian discussed above.

The form we have chosen for the interion Hamiltonian in Eq. (5) allows us to write down the following expression for the molecular field h_{MF} in Eq. (3):

$$\mathcal{H}_{MF} = h_{MF}J_z = 2z\mathcal{J}\langle J_z\rangle J_z,$$

where z is the number of nearest neighbors, $\mathcal{J}$ is the scalar magnetic exchange in Eq. (5), and $\langle J_z\rangle$ is the expectation value of the statically ordered magnetic moment on a given Ce^{3+} site. This time reversal symmetry breaking term in the single-ion Hamiltonian will split the three Kramers doublets illustrated in Fig. 4. We will discuss the effects of this term below in detail in the context of the single-ion susceptibility.

C. Green's functions and relation to neutron scattering

The energy eigenstates of the single-ion Hamiltonian discussed can be used to directly calculate the neutron scattering response measured in experiment. We summarize the approach we have taken here with a full description given in the Appendix. We note that this methodology has been outlined in several previous papers by us [37,49,56–59]. We calculate the Green's function ($G^{\alpha\beta}(\mathbf{q}, \omega)$, with $\alpha\beta$ denoting Cartesian coordinates) response which is related to the neutron scattering cross section [by the structure factor $S^{\alpha\beta}(\mathbf{q}, \omega)$] by the fluctuation-dissipation theorem,

$$S^{\alpha\beta}(\mathbf{q}, \omega) = -\frac{1}{\pi}\frac{1}{1 - \exp(\omega/k_B T)}\Im G^{\alpha\beta}(\mathbf{q}, \omega). \tag{6}$$

The Green's function, in the local rotating frame, $\tilde{G}^{\alpha\beta}(\mathbf{q}, \omega)$, in the case of the interaction Hamiltonian stated in Eq. (5) is given by the Dyson equation (in the rotating frame denoted via "~" discussed in the Appendix),

$$\underline{\tilde{G}}(\mathbf{q}, \omega) = \underline{g}(\omega) + \underline{g}(\omega)\underline{\tilde{\mathcal{J}}}(\mathbf{q})\underline{\tilde{G}}(\mathbf{q}, \omega). \tag{7}$$

The single site susceptibility $g^{\alpha\beta}(\omega)$, where only the ground state $|0\rangle$ is populated and there are no thermally
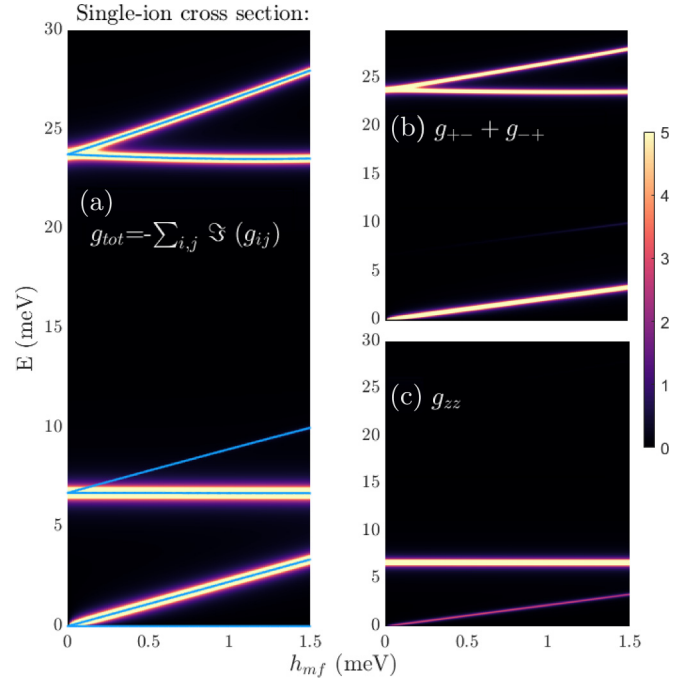

FIG. 5. The single ion susceptibility plotted as a function of molecular field in the single-ion Hamiltonian Eq. (4). (a) illustrates the sum over all matrix elements $g^{\alpha\beta}(\omega)$ and the anisotropy is illustrated (b) and (c), which plots in-plane and out-of-plane components, respectively. The blue lines in (a) are the energy eigenvalues, whereas g lacks intensity despite an energy eigenvalue implies the excitations to that mode are not allowed by dipole selection rules of neutron scattering.

excited states (low temperature $T \to 0$ limit), is defined as

$$g^{\alpha\beta}(\omega) = \sum_n \frac{\langle 0|J^\alpha|n\rangle\langle n|J^\beta|0\rangle}{\omega + i\Gamma - (\omega_n - \omega_0)} - \frac{\langle n|J^\alpha|0\rangle\langle 0|J^\beta|n\rangle}{\omega + i\Gamma + (\omega_n - \omega_0)} \tag{8}$$

with $|n\rangle$ the eigenstates of the single-ion Hamiltonian with energies $\hbar\omega_n$.

The single-site susceptibility provides the foundation for calculating the neutron scattering response with the single-ion states coupled through the exchange Hamiltonian. The local crystalline electric field imposes an underlying anisotropy to the magnetic response. This is shown by plotting the total single site response ($= \sum_{\alpha\beta} g^{\alpha\beta}$) as a function of the molecular field term in the Hamiltonian [Eq. (3)] which breaks time-reversal symmetry and hence Zeeman splits the three single-ion doublets (5).

One advantage of the Green's function approach is that anisotropy is built into the single-ion response ($g^{\alpha\beta}$) originating from the crystalline electric field Hamiltonian. The full anisotropic single-site susceptibility takes the following matrix form in Cartesian coordinates:

$$\underline{\underline{g}}(\omega) = \begin{bmatrix} g^{xx} & g^{xy} & g^{xz} \\ g^{yx} & g^{yy} & g^{yz} \\ g^{zx} & g^{zy} & g^{zz} \end{bmatrix}.$$

The total single-ion response (g_{tot}) is plotted in Fig. 5(a). The in-plane components ($g^{xx} + g^{yy}$) and out of plane

components (g^{zz}) are plotted in Figs. 5(b) and 5(c) as a function of h_{MF} which breaks the doublet degeneracy. We discuss the value of h_{MF} below. The single-ion response displays anisotropy with differing excitations (particularly at ~ 5 meV) for in-plane ($g^{xx} + g^{yy}$) and out-of-plane (g^{zz}) components. Owing to the anisotropy from the crystalline electric field, the single-ion response is very anisotropic and we will show below that this translates into a spatially anisotropic multimode response in the neutron cross section.

With the single site susceptibility discussed, the total neutron cross section can be calculated from the Green's function response by solving the Dyson equation Eq. (8):

$$\underline{\tilde{\underline{G}}}(\mathbf{q}, \omega) = \underline{g}(\omega)[\underline{\underline{1}} - \underline{\tilde{\underline{\mathcal{J}}}}(\mathbf{q})\underline{g}(\omega)]^{-1}.$$

Through taking the imaginary part of this matrix equation and transforming back to the laboratory frame from the local rotating frame (see the Appendix), the total neutron cross section can be calculated.

D. Comparison with SU(N) spin-wave theory

The application of Green's functions to neutron scattering involves two key steps. First, the calculation of the single-site eigenstates based on a local crystalline electric and molecular field Hamiltonian. The symmetry of these states satisfies a discrete C_4 symmetry imposed by the local tetragonal point group symmetry as the three Stevens' operators that define the local crystalline electric field are invariant under the four symmetry operators (which includes the identity) of the C_4 group. The second step of our excitonic model is to couple these single-ion eigenstates through the RPA.

We compare this to the general SU(N) spin-wave theory [42] which has been previously applied in several compounds including spin-dimer compounds [41] and also in materials where spin-orbit coupling is relevant [60–62]. Theoretically, our excitonic approach and SU(N) give the same results. However, there are several differences in the starting point of these theoretical analyses which we outline. In the case of Ce^{3+}, there are six basis states corresponding to eigenstates of the observable operator J_z. The rotation matrix that rotates from the N many $|j, m\rangle$ states to those of the crystal field Hamiltonian belongs to the SU($N \equiv 6$) group. Semiclassical coherent states [63–67], which locally [68] have continuous SU(N) symmetry, are then constructed to describe the members of the six-dimensional basis. We note that SU($N \equiv 6$) requires the identity (Casimir) and N^2-1 (35) generators of symmetry which form the continuous Lie group and hence can be used to describe multipolar excitations. An arbitrary local order parameter is always contained in the most general SU(N) order parameter with N^2-1 components. Recent examples of applications of this can be found in Ref. [69].

SU(N) and our Green's function method aim to move beyond standard spin-wave theory which is based on a starting symmetry of SU(2), like outlined above for the effective $S = \frac{1}{2}$ description of CeRhIn$_5$. While the interaction Hamiltonian $\mathcal{H}_{\text{inter}}$ has SU(2) symmetry with the generators of the Lie algebra being $J_{x,y,z}$, our excitonic approach applying Green's functions forces the local discrete C_4 symmetry as it applies
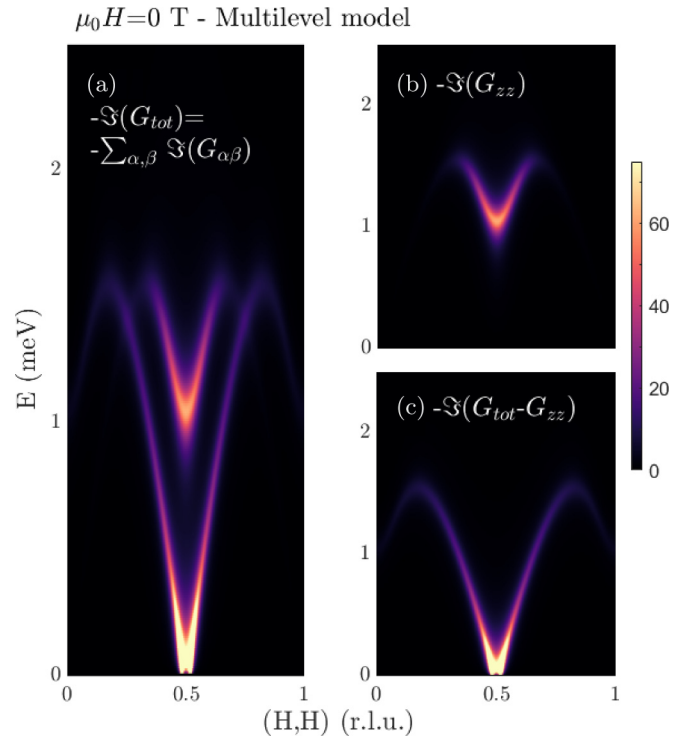

FIG. 6. The calculated $\mu_0 H = 0$ T neutron response. (a) displays the total cross section and (b) and (c) display the in-plane out and out of plane components. The parameters used for this calculation include the crystalline electric field parameters listed in Table II, $\mathcal{J} = 0.135$ meV, and $h_{MF} = 0.63$ meV (discussed in the text).

eigenstates of the Stevens' operators that are invariant under the local point group. We will show below this naturally builds in anisotropy into the predicted excitations. As illustrated in our previous works [49] it also allows a direct connection between measurable parameters and physical quantities (such as spin-orbit coupling in the context of transition metal ions).

In the approach below we apply the excitonic Green's response function methodology to this problem and do not use the generalized pseudoboson coherent state methodology of SU(N). In our case the single-ion eigenstates of the local discrete point group are used as a starting basis and then subsequently coupled through the RPA outlined above and provided more in detail in the Appendix.

V. THEORETICAL NEUTRON RESULTS

We calculate the full neutron response for CeRhIn$_5$ in Fig. 6 at $\mu_0 H = 0$ T. We use the values listed in Table II for the Stevens' parameters to describe the crystalline electric field. We have tweaked $\mathcal{J} = 0.135$ meV to match the dispersion bandwidth observed in experiment. We note that previous $S_{\text{eff}} = \frac{1}{2}$ models predict a much larger exchange constant of ~ 0.7–0.9 meV [33,35]. However, given that we are considering a full $j = \frac{5}{2}$ model the value for the exchange quoted here should be scaled by a factor of 5, making it in agreement with previous estimates. For the molecular field component of the single-ion Hamiltonian, given that the z axis is defined through the electrostatic field and the magnetic moments order within the $a - b$ plane, we have taken the case

of the molecular field to be along x. The molecular field h_{MF} depends on the expectation value $\langle J_{\bar{z}} \rangle$ which is related to the ordered magnetic moment found in neutron diffraction via $\mu = g_J \langle J_{\bar{z}} \rangle \mu_B$, with $g_J = \frac{6}{7}$ for Ce^{3+}. The ordered magnetic moment for $CeRhIn_5$ has been reported to be significantly reduced over expectations based on an isolated Ce^{3+} with values of $\sim 0.4\,\mu_B$ being found [70,71]. We note that in other Ce^{3+}-based compounds such as $CeIn_3$ [72,73] and Ce_2RhIn_8 [74] the ordered magnetic moment is reported to be $\mu \sim 0.5\,\mu_B$. We can also estimate the ordered moment based on the crystalline electric field Stevens' parameters listed in Table II:

$$g_J |\langle 0 | J_{\bar{z}} | 0 \rangle| \mu_B = 0.49 \mu_B.$$

This is in good agreement with the values reported for Ce^{3+} heavy fermion compounds. For the purposes of our calculation we have taken an ordered moment of $\mu = 0.5 \mu_B$ and therefore $h_{MF} = \frac{\mu}{g_J \mu_B} \times 2 \times z \times \mathcal{J} = 0.63\,\text{meV}$ (with $z = 4$ for the number of nearest neighbors in the $a - b$ plane).

The calculation predicts two excitations (Fig. 6) with one being energetically gapless and corresponding to fluctuations within the $a - b$ plane and a second energetically gapped for excitations out of the plane or along the crystallographic c axis. The gapless excitation is required owing to the presence of a continuous symmetry related to rotating the Ce^{3+} moments within the $a - b$ plane. This is in qualitative agreement with neutron spectroscopy results for the energetically well defined portion of the neutron response [33,35]. The use of excitations from single-ion states incorporates the anisotropy of the lattice and this is reflected in the neutron scattering response and our Green's function calculations. We note the presence of two distinct modes is consistent with a symmetry analysis of the magnetic ground state which, based on the space group $P4/m\,2/m\,2/m$ (No. 123) results in two irreducible representations. One has two basis vectors within the crystallographic $a - b$ plane and a second irreducible representation which as a single vector along c [33].

The calculated neutron response in an applied field within the crystallographic $a - b$ plane is shown in Fig. 7. We have tuned $\mathcal{J} = 0.03\,\text{meV}$ so that dispersing band width of the excitation matches the data taken at $\mu_0 H = 9\,\text{T}$ from MACS in Figs. 3(c) and 3(f). We have then fixed the molecular field based on $\mathcal{J}$ to be $h_{MF} = 0.14\,\text{meV}$. The applied field along the $[1\bar{1}0]$ is included as an additional Zeeman term analogous to the molecular field,

$$\mathcal{H}_{Zeeman} = \alpha g_J \mu_B H \frac{(J_x + J_y)}{\sqrt{2}}.$$

We have included a heuristic screening term of $\alpha = 0.88$ to account for screening of the magnetic field and field inhomogeneities or misalignment of the magnetic field. This term was tuned so that the in-plane excitation appears at $\sim 1\,\text{meV}$. The model reproduces the decrease in bandwidth and the enhanced gap with an applied magnetic field and indicates that the apparent increase in anisotropy with applied field is Zeeman driven. The connection between this increase in anisotropy and and large field ($\sim 28\,\text{T}$) field-induced density waves [75] is not clear from this current comparatively low-field study, however the anisotropy gap in the 115 heavy fermion system is important for tuning the ground state [76]. Interestingly, the model here also predicts a weakening of the
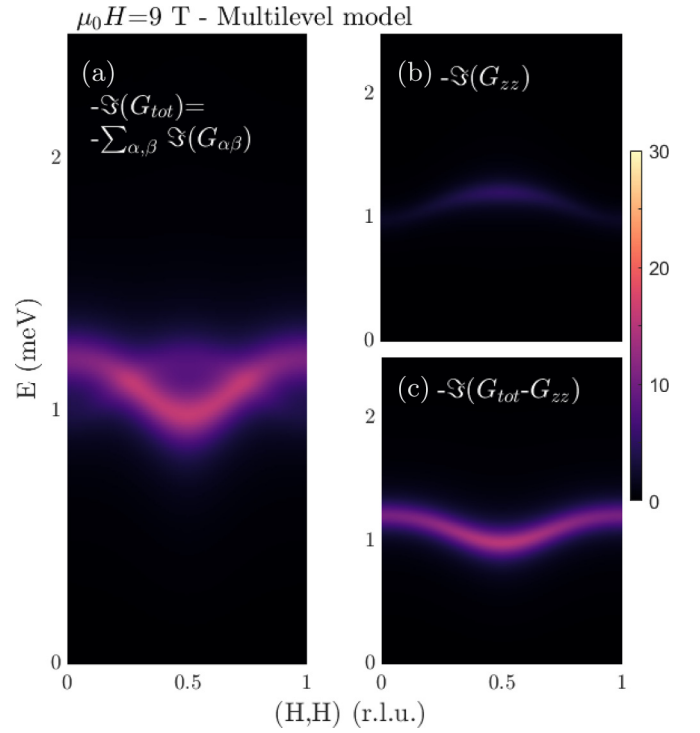

FIG. 7. The calculated $\mu_0 H = 9\,\text{T}$ neutron response. (a) displays the total cross section and (b) and (c) display the in-plane out and out of plane components. The parameters used for this calculation include the crystalline electric field parameters listed in Table II, $\mathcal{J} = 0.03\,\text{meV}$, and $h_{MF} = 0.14\,\text{meV}$ (discussed in the text).

the mode polarized along the crystallographic c axis. This could provide the origin of the fact that this mode was not observable on MACS at small values of momentum transfers along the c axis in our experiments.

VI. DISCUSSION AND CONCLUSIONS

In summary, we have applied a general multilevel spin wave model using Green's functions to calculate the neutron scattering response. This approach brings in anisotropic crystalline electric field Stevens' operators based on the discrete C_4 local point group and the coupling terms via dipole operators in the magnetic Hamiltonian. This mean-field theory describes the two excitations observed with neutron scattering and also their differing polarization at zero applied field and also can be used to heuristically understand the applied magnetic field dependence.

In terms of zero field results, the low-energy mode is the gapless Goldstone mode required from the presence of a continuous symmetry of the helical magnetic structure. Indeed, the entire magnetic structure is symmetric for two-dimensional rotations in the $a - b$ plane. This corresponds to O(2) operators commuting with the magnetic Hamiltonian. However, experimentally there has been the suggestion of a gap in this response. While higher resolution data maybe required to fully confirm this, it is possible that other processes like order-disorder, defects, or crystal field fluctuations maybe the origin [77]. These are not accounted for in our mean-field excitonic model.

It is interesting to relate these excitations to those observed in isostructural superconducting counterparts like $CeCoIn_5$. To our knowledge, in superconducting compounds there has not been a report of temporally well defined (underdamped) spin excitations *polarized* within the crystallographic $a-b$ plane either in superconducting or nonsuperconducting normal phases. However, excitations polarized along the crystallographic c axis have been reported in Hg-doped $CeCoIn_5$ [78] being a precursor to magnetic order [79]. Similar static results have been reported for those Cd doped [80,81]. No in-plane excitations were observable in the neutron experiments. Notably, the spin resonance found in superconducting and paramagnetic $CeCoIn_5$ was found to also be anisotropic and polarized along the crystallographic c axis. Comparing antiferromagnetic $CeRhIn_5$ with isostructural superconducting $CeCoIn_5$ seems to indicate robustness of magnetic excitations polarized along the crystallographic c axis in comparison to the in-plane $a-b$ plane fluctuations.

The resonance mode has been found to disperse in momentum leading to the suggestion that it may not originate from a d-wave superconducting order parameter but rather to the removal of decay channels that cause dampening and hence broadening in energy [82,83]. This "magnon" scenario has also been suggested theoretically [84]. Also noteworthy is that the single-ion framework would predict magnetic excitations in the absence of a time reversal symmetry breaking field to be doublets owing to Kramers' theorem. This is also reported in experiment for the spin resonance where the splitting of this doublet resonance with a field can be used to condense a static spin-density wave "Q phase" [85–88]. However, we note that idea of attributing the resonance to a magnon has a problem in our current framework described above to model the excitations in $CeRhIn_5$. The gapping of the mode originates from a time reversal symmetry breaking field (here the molecular field). This is not the case for the $CeCoIn_5$ resonance as such a situation would not result in a doublet which seems to imply via Kramers theorem that time reversal symmetry is preserved. The d-wave superconducting order parameter or the magnon description of the resonance still needs further theoretical work.

The instability of the in-plane magnetic excitations is also seen in parent $CeRhIn_5$ (illustrated in Fig. 3) where these excitations are found to coexist with a momentum and energy broadened component that is reminiscent of multimagnon processes reported in insulating model magnets. This indicates an apparent instability of in-plane excitations in comparison to out-of-plane components. The origin of this instability and also the apparent stability of c-axis magnetic excitations will require further theoretical work along with their link to superconductivity as displayed by the observation of a c-axis polarized spin resonance in $CeCoIn_5$.

In conclusion, we have analyzed the magnetic excitations in $CeRhIn_5$ in terms of a mean-field excitonic model constrained by the local C_4 point group symmetry. This captures the anisotropy resulting in two magnetic modes with differing polarization, in agreement with experiment. We then discuss this framework in the context of an applied magnetic field which controls the local single-site anisotropy.

ACKNOWLEDGMENTS

APPENDIX: GREEN'S FUNCTIONS AND NEUTRON SCATTERING

In this Appendix, we outlined the Green's function approach in detail.

1. Green's functions

Having defined the basis states built from single-ion physics and the Hamiltonian for interactions in the main paper, we discuss in this Appendix the calculation of neutron scattering intensities and the coupling of these single-ion states at a mean-field level. To accomplish this we apply the Green's function [89] formalism for neutron scattering.

The technique for applying Green's functions to neutron spectroscopy data has been outlined in several papers by us in the context of spin-orbit coupling and $3d$ transition metal ions. We take the same approach here, but with a differently defined single-ion Hamiltonian which determines the eigenstates that are coupled at a mean-field level. Our initial studies investigated collinear magnetically ordered compounds, such as spin-orbit coupling in CoO. More recently we have generalized this approach to noncollinear compounds and reduced the number of equations that are required for the calculations. We have further demonstrated the equivalence with conventional spin-wave theory, such as can be applied in *SpinW* [90], through studying compounds which lack an orbital degree of freedom and have spin-only magnetic moments. In the formalism that follows, we assume one magnetic ion per unit cell, taking advantage of the rotating frame, and that we are at low temperatures where the excited levels are not thermally populated.

We will merely summarize the key calculation results here, but for more details see Ref. [91]. In this analysis we make use of summation notation requiring multiple sets of indices corresponding to different entities and also different labeling of operators. In Table III we define our notation.

The neutron scattering cross section is directly proportional to the structure factor $S(\mathbf{q}, \omega)$

$$S(\mathbf{q}, \omega) = g_L^2 f^2(\mathbf{q}) \sum_{\alpha\beta} (\delta_{\alpha\beta} - \hat{q}_\alpha \hat{q}_\beta) S^{\alpha\beta}(\mathbf{q}, \omega),$$

where g_L is the Landé factor and $f(\mathbf{q})$ is the Ce^{3+} magnetic form factor. The summation is over $\alpha, \beta = x, y, z$ and

$$S^{\alpha\beta}(\mathbf{q}, \omega) = \frac{1}{2\pi} \int dt e^{i\omega t} \langle J^\alpha(\mathbf{q}, t) J^\beta(-\mathbf{q}, 0)\rangle.$$

TABLE III. Summary of labeling convention for indices and notation.

Index	Description
$i, j,..$	Unit cell position indices
$\alpha, \beta, \mu, \nu,...$	Cartesian coordinates (x, y, z)
$\underline{X}$	Matrix quantities
$A, B, C, ...$	Quantities in laboratory frame
$\tilde{A}, \tilde{B}, \tilde{C}, ...$	Quantities in local rotating frame
J_i	Angular momentum observables
$\mathcal{J}$	Symmetric (scalar) Heisenberg exchange

The relation to the Green's response function which can be directly connected with the neutron scattering intensity via the fluctuation-dissipation theorem is given by

$$S^{\alpha\beta}(\mathbf{q}, \omega) = -\frac{1}{\pi} \frac{1}{1 - \exp(\omega/k_B T)} \Im G^{\alpha\beta}(\mathbf{q}, \omega) \quad \text{(A1)}$$

with T the temperature k_B the Boltzmann factor. The Green's function here is defined in terms of the commutator of the angular momentum observables

$$G_{i,j}^{\alpha\beta}(t) = -i\Theta(t)\langle[J_i^\alpha(t), J_j^\beta(0)]\rangle$$

with the Heaviside function $\Theta(t)$ forcing causality. Through taking a time derivative of the Green's function, an equation of motion can be derived which depends on the commutator of the angular momentum operators with the magnetic Hamiltonian discussed above. These commutators are discussed in previous references and after applying a mean field decoupling scheme [50], the following expression for the Green's function can be derived:

$$G_{i,j}^{\alpha\beta}(\omega) = g^{\alpha\beta}(\omega)\delta_{ij}$$
$$+ \sum_\nu \sum_k g^{\alpha\nu}(\omega)\mathcal{J}_{ik}G_{kj}^{\nu\beta}(\omega). \quad \text{(A2)}$$

The single site susceptibility $g^{\alpha\beta}(\omega)$, where only the ground state is populated and there are no thermally excited states (low temperature $T \to 0$ limit), is defined as

$$g^{\alpha\beta}(\omega) = \sum_n \frac{\langle 0|J^\alpha|n\rangle\langle n|J^\beta|0\rangle}{\omega + i\Gamma - (\omega_n - \omega_0)}$$
$$- \frac{\langle n|J^\alpha|0\rangle\langle 0|J^\beta|n\rangle}{\omega + i\Gamma + (\omega_n - \omega_0)}, \quad \text{(A3)}$$

where Γ is required to ensure analyticity and can be physically interpreted as an energy linewidth from the spectrometer resolution. The summation over the states $|n\rangle$ which are the eigenstates of the single-ion Hamiltonian discussed above.

We note that Eq. (A3) has the form of the Dyson equation with the single site susceptibility having the role of the bare propagator and the second term a first-order perturbative correction [91]. Indeed, the Dyson equation [Eq. (A3)] can then be written more compactly in matrix form which allows Cartesian coordinates to be included implicitly while summations and indices are only over unit cells. Using matrix notation, the Dyson equation in terms of atomic coordinates ij and frequency ω takes the form

$$\underline{\underline{G}}_{i,j}(\omega) = \underline{\underline{g}}(\omega)\delta_{ij} + \sum_k \underline{\underline{g}}(\omega)\underline{\underline{\mathcal{J}}}_{ik}\underline{\underline{G}}_{kj}(\omega).$$

The Heisenberg coupling here, while written as a matrix, will be approximated as proportional to the 3×3 identity, $\underline{\underline{\mathcal{J}}}_{ik} \equiv \mathcal{J}_{ik}\underline{\underline{1}}$, where $\mathcal{J}_{ik}$ is a scalar. Our Dyson-equation is an equation of motion for a quasiparticle describing excitations between single-ion states in a crystalline electric field.

2. Rotating frame for incommensurate magnetic structures

The above description for the Green's functions was cast in terms a single magnetic site per unit cell. However, in the case of CeRhIn$_5$ the magnetic structure is incommensurate resulting from a helical (within the $a - b$ plane) magnetic structure with a periodicity along the $c -$ axis defined by the propagation wave vector $\vec{Q}_0 = (\frac{1}{2}, \frac{1}{2}, 0.297)$. Given the extended nature of the magnetic unit cell, it is not possible to define a crystallographic basis that can be translated and the incommensurate nature of the magnetic structure results in the magnetic ion in each unit cell having a unique single site susceptibility ($\underline{\underline{g}}(\omega)$). To circumvent this problem and avoid using large unit cells which are cumbersome for calculations, we therefore utilize a rotating frame formalism which allows us to work in the primitive unit cell and also considerably reduces the number of equations required to be solved numerically. In this approach, we move to a reference frame that rotates with the magnetic structure $(\tilde{x}, \tilde{y}, \tilde{z})$ with the magnetic moment oriented along $\tilde{z}$ in its local reference frame. This process has been outlined in general in Ref. [56] for the case of RbFe^{2+}Fe^{3+}F$_6$. To apply this, we need to define a rotation matrix that rotates this local coordinate system from one Ce^{3+} site to another. This is most conveniently done utilizing Rodrigues' rotation formula which allows rotation matrices to be constructed from the propagation wave vector (in this case $\mathbf{Q} = (0.5, 0.5, 0.297)$). The rotation matrix for a site at a position $\mathbf{r_i}$ can be written

$$\underline{\underline{R}}_i = e^{i\mathbf{Q}\cdot\mathbf{r}_i}\underline{\underline{\Phi}} + e^{-i\mathbf{Q}\cdot\mathbf{r}_i}\underline{\underline{\Phi}}^* + \mathbf{n}\mathbf{n}^T, \quad \text{(A4a)}$$

$$\underline{\underline{\Phi}} = \frac{1}{2}(\underline{\underline{1}} - \mathbf{n}\mathbf{n}^T - i\underline{\underline{[n]}}_\times), \quad \text{(A4b)}$$

where $\mathbf{n}$ is a vector normal to the plane of the spiral (in the case of CeRhIn$_5$ this is $\mathbf{n} = (0, 0, 1)^T$). In matrix form

$$\underline{\underline{[n]}}_\times = \begin{bmatrix} 0 & -n_k & n_j \\ n_k & 0 & -n_i \\ -n_j & n_i & 0 \end{bmatrix}.$$

Using the Eqs. (A4a) and (A4b) to define a rotation matrix for each site, we can define a rotation matrix for sites ij and write the Dyson equation for the Green's function $\tilde{G}$ in the rotating

frame

$$\underline{\underline{\tilde{G}}}_{i,j}(\omega) = \underline{\underline{R}}_i^T \underline{\underline{G}}_{i,j}(\omega) \underline{\underline{R}}_j = \underline{\underline{g}}(\omega)\delta_{ij}\dots$$
$$+ \sum_k \underline{\underline{g}}(\omega)\left(\underline{\underline{R}}_i^T \underline{\underline{\mathcal{J}}}_{ik} \underline{\underline{R}}_k\right)\left(\underline{\underline{R}}_k^T \underline{\underline{G}}_{kj}(\omega) \underline{\underline{R}}_j\right),$$

where we have used the unitary property of rotation matrices $\underline{\underline{R}}_k \underline{\underline{R}}_k^T \equiv \underline{\underline{1}}$. We have also used the approximation that the rotation matrices ($\underline{\underline{R}}_i$) commute with the single-ion susceptibility matrices $\underline{\underline{g}}(\omega)$ [92]. This approximation will be discussed and quantified below in the context of the specific case of CeRhIn$_5$. Putting this all together and collecting the terms in brackets, we can write the Dyson equation in the rotating frame as

$$\underline{\underline{\tilde{G}}}_{i,j}(\omega) = \underline{\underline{g}}(\omega)\delta_{ij} + \sum_k \underline{\underline{g}}(\omega)\underline{\underline{\tilde{\mathcal{J}}}}_{ik}\underline{\underline{\tilde{G}}}_{kj}(\omega).$$

Note we have used the notation that all quantities written in the rotation frame have a "tilde" (for example $\underline{\underline{\tilde{G}}}$ or $\underline{\tilde{J}}$) above them. Taking the Fourier transform and switching from index notation to matrix notation (for example $G^{\alpha\beta} \rightarrow \underline{\underline{G}}$) gives

$$\underline{\underline{\tilde{G}}}(\mathbf{q}, \omega) = \underline{\underline{g}}(\omega) + \underline{\underline{g}}(\omega)\underline{\underline{\tilde{\mathcal{J}}}}(\mathbf{q})\underline{\underline{\tilde{G}}}(\mathbf{q}, \omega). \tag{A5}$$

Regarding the Fourier transform of the exchange term $\underline{\underline{\mathcal{J}}}$ which couples differing magnetic Ce^{3+} sites, we define $\underline{\underline{\mathcal{J}}}$ as

$$\underline{\underline{\mathcal{J}}}(\mathbf{q}) = \sum_{mn} \underline{\underline{\mathcal{J}}}_{mn} e^{-i\mathbf{q}\cdot(\mathbf{r}_m - \mathbf{r}_n)}, \tag{A6}$$

where $\underline{\underline{\mathcal{J}}}_{mn}$ is the exchange coupling between Ce^{3+} sites at positions $\mathbf{r}_m$ and $\mathbf{r}_n$. Incorporating the rotation matrices into the definition of $\underline{\underline{\mathcal{J}}}$ in the Dyson equation allows the exponential factors in the rotation matrices to be incorporated into $\tilde{J}(\mathbf{q})$ as follows:

$$\underline{\underline{\mathcal{J}}}(\mathbf{q}) \rightarrow \underline{\underline{\tilde{\mathcal{J}}}}(\mathbf{q}) = \underline{\underline{\mathcal{J}}}(\mathbf{q}+\mathbf{Q})\underline{\underline{\Phi}} + \underline{\underline{\mathcal{J}}}(\mathbf{q}-\mathbf{Q})\underline{\underline{\Phi}}^* + \underline{\underline{\mathcal{J}}}(\mathbf{q})\mathbf{n}\mathbf{n}^T.$$

The compact form of $\underline{\underline{\tilde{G}}}(\mathbf{q}, \omega)$ that is now Fourier transformed and written in terms of matrices can be readily solved

$$\underline{\underline{\tilde{G}}}(\mathbf{q}, \omega) = \underline{\underline{g}}(\omega)[\underline{\underline{1}} - \underline{\underline{\tilde{\mathcal{J}}}}(\mathbf{q})\underline{\underline{g}}(\omega)]^{-1}.$$

Note that this equation is still in the rotating frame. To transform to the laboratory frame so that we can obtain the original Green's function from which we can calculate the neutron scattering response, we rotate back as follows:

$$\underline{\underline{G}}(\mathbf{q}, \omega) = \mathbf{n}\mathbf{n}^T \underline{\underline{\tilde{G}}}(\mathbf{q}, \omega)\mathbf{n}\mathbf{n}^T + \Phi^* \underline{\underline{\tilde{G}}}(\mathbf{q}+\mathbf{Q}, \omega)\Phi^T$$
$$+ \Phi\underline{\underline{\tilde{G}}}(\mathbf{q}-\mathbf{Q}, \omega)\Phi^{*T}.$$

Note that $\Phi^{*T} \equiv \Phi^\dagger$, however, we have kept complex conjugate transpose for consistency of notation and to avoid confusion between the transpose and the Hermitian conjugate (or adjoint). This approach differs slightly from our previous work with CoO where we solved a set of linear equations for the various components of G and the incorporation of the rotating frame allows us to combine all of the various sites in the lattice into one single RPA equation for the Green's function response. Above in the main text, we applied this to the case of CeRhIn$_5$.
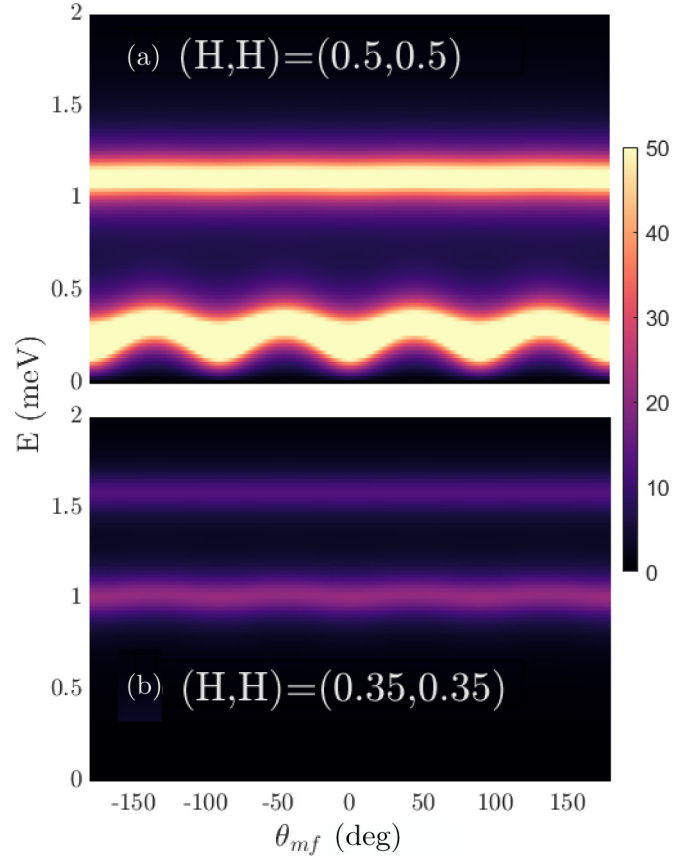

FIG. 8. Plots of the calculated neutron scattering intensity as a function of angle within the $a-b$ plane of the molecular field. This illustrates the effects of the approximation that the rotation matrix commutes with the single-ion susceptibility ($[\underline{\underline{g}}(\omega), \underline{\underline{R}}_i] \equiv 0$) discussed in the main text.

3. Rotating frame approximations

An approximation applied above when moving to the rotating frame was that the rotation matrices commuted with the single-ion susceptibility ($[\underline{\underline{g}}(\omega), \underline{\underline{R}}_i] \equiv 0$). Under a rotation transformation, this left the first term in the Dyson expansion unchanged while allowed us to commute the rotation matrix to surround the exchange term $\mathcal{J}$. It is not clear if this approximation is appropriate given the very anisotropic crystal field terms for Ce^{3+} in CeRhIn$_5$ and the complexity of the Stevens' operators required by symmetry. We also note that unlike transition metal ion counterparts where the crystal field terms are several orders of magnitude larger than exchange energetics, the anisotropic crystal field terms and exchange parameters are of similar sizes in the rare earth $4f$ elements.

We investigate the limits of this approximation in Fig. 8. In this calculation we have chosen two momentum positions at the magnetic zone center $\mathbf{q} = (0.5, 0.5)$ and away from the zone center near the peak of the dispersion at $\mathbf{q} = (0.35, 0.35)$. In this figure we have rotated the molecular field within the $a-b$ plane (denoted as θ_{mf}). To give an energetic gap to the lowest energy mode, we have arbitrarily chosen this calculation with a slightly larger $h_{MF} = 0.65$ meV

over the value of 0.63 meV motivated above. While there is a small ~ 0.1 meV variation in the low-energy excitation polarized within the $a - b$ plane, the rotation does not change the number of modes, or the energy scale in comparison to the overall bandwidth of the excitations. We therefore use this plot as justification for commuting the rotation matrices through the single-ion susceptibility $g(\omega)$ at the mean-field level above in the Dyson equation.

[1] G. R. Stewart, Heavy-fermion systems, Rev. Mod. Phys. **56**, 755 (1984).

[2] N. D. Mathur, F. M. Grosche, S. R. Julian, I. R. Walker, D. M. Freye, R. K. W. Haselwimmer, and G. G. Lonzarich, Magnetically mediated superconductivity in heavy fermion compounds, Nature (London) **394**, 39 (1998).

[3] C. Pfleiderer, Superconducting phases of f-electron compounds, Rev. Mod. Phys. **81**, 1551 (2009).

[4] C. Proust and L. Taillefer, The remarkable underlying ground states of cuprate superconductors, Annu. Rev. Condens. Matter Phys. **10**, 409 (2019).

[5] K. M. Shen and J. C. S. Davis, Cuprate high-T_c superconductors, Mater. Today **11**, 14 (2008).

[6] M. A. Kastner, R. J. Birgeneau, G. Shirane, and Y. Endoh, Magnetic, transport, and optical properties of monolayer copper oxides, Rev. Mod. Phys. **70**, 897 (1998).

[7] D. C. Johnston, The puzzle of high temperature superconductivity in layered iron pnictides and chalcogenides, Adv. Phys. **59**, 803 (2010).

[8] P. Dai, Antiferromagnetic order and spin dynamics in iron-based superconductors, Rev. Mod. Phys. **87**, 855 (2015).

[9] H. Sun, M. Huo, X. Hu, J. Li, Z. Liu, Y. Han, L. Tang, Z. Mao, P. Yang, B. Wang, J. Cheng, D.-X. Yaho, and G.-M. Zhang, Signatures of superconductivity near 80 k in a nickelate under high pressure, Nature (London) **621**, 493 (2023).

[10] P. C. Canfield, P. L. Gammel, and D. J. Bishop, New magnetic superconductors: A toy box for solid-state physicists, Phys. Today **51**, 40 (1998).

[11] K. H. Muller and V. N. Narozhnyi, Interaction of superconductivity and magnetism in borocarbide superconductors, Rep. Prog. Phys. **64**, 943 (2001).

[12] M. W. Haverkort, A. Tanaka, L. H. Tjeng, and G. A. Sawatzky, Nonresonant inelastic x-ray scattering involving excitonic excitations: The examples of NiO and CoO, Phys. Rev. Lett. **99**, 257401 (2007).

[13] B. C. Larson, W. Ku, J. Z. Tischler, C.-C. Lee, O. D. Restrepo, A. G. Eguiluz, P. Zschack, and K. D. Finkelstein, Nonresonant inelastic x-ray scattering and energy-resolved Wannier function investigation of $d - d$ excitations in NiO and CoO, Phys. Rev. Lett. **99**, 026401 (2007).

[14] R. A. Cowley, W. J. L. Buyers, C. Stock, Z. Yamani, C. Frost, J. W. Taylor, and D. Prabhakaran, Neutron scattering investigation of the $d - d$ excitations below the Mott gap of CoO, Phys. Rev. B **88**, 205117 (2013).

[15] Y.-J. Kim, A. P. Sorini, C. Stock, T. G. Perring, J. van den Brink, and T. P. Devereaux, Probing high-energy electronic excitations in NiO using inelastic neutron scattering, Phys. Rev. B **84**, 085132 (2011).

[16] C. Petrovic, P. G. Pagliuso, M. F. Hundley, R. Movshovich, J. L. Sarrao, J. D. Thompson, Z. Fisk, and P. Monthoux, Heavy-fermion superconductivity in CeCoIn₅, J. Phys.: Condens. Matter **13**, L337 (2001).

[17] K. Izawa, H. Yamaguchi, Y. Matsuda, H. Shishido, R. Settai, and Y. Onuki, Angular position of nodes in the superconducting gap of quasi-2D heavy-fermion superconductor CeCoIn₅, Phys. Rev. Lett. **87**, 057002 (2001).

[18] H. Aoki, T. Sakakibara, H. Shishido, R. Settai, Y. Onuki, P. Miranovic, and K. Machida., Field-angle dependence of the zero-energy density of states in the unconventional heavy-fermion superconductor CeCoIn₅, J. Phys.: Condens. Matter **16**, L13 (2004).

[19] J. D. Thompson and Z. Fisk, Progress in heavy-fermion superconductivity: Ce115 and related materials, J. Phys. Soc. Jpn. **81**, 011002 (2012).

[20] T. Park, H. Lee, I. Martin, X. Lu, V. A. Sidorov, K. Gofryk, F. Ronning, E. D. Bauer, and J. D. Thompson, Textured superconducting phase in the heavy fermion CeRhIn₅, Phys. Rev. Lett. **108**, 077003 (2012).

[21] C. Stock, C. Broholm, J. Hudis, H. J. Kang, and C. Petrovic, Spin resonance in the d-wave superconductor CeCoIn₅, Phys. Rev. Lett. **100**, 087001 (2008).

[22] O. Stockert, J. Arndt, E. Faulhaber, C. Geibel, H. S. Jeevan, S. Kirchner, M. Loewenhaupt, K. Schmalzl, W. Schmidt, Q. Si, and F. Steglich, Magnetically driven superconductivity in CeCu₂Si₂, Nat. Phys. **7**, 119 (2011).

[23] I. Eremin, G. Zwicknagl, P. Thalmeier, and P. Fulde, Feedback spin resonance in superconducting CeCu₂Si₂ and CeCoIn₅, Phys. Rev. Lett. **101**, 187001 (2008).

[24] S. Raymond and G. Lapertot, Ising incommensurate spin resonance of CeCoIn₅: A dynamical precursor of the Q phase, Phys. Rev. Lett. **115**, 037001 (2015).

[25] C. Stock, C. Broholm, Y. Zhao, F. Demmel, H. J. Kang, K. C. Rule, and C. Petrovic, Magnetic field splitting of the spin resonance in CeCoIn₅, Phys. Rev. Lett. **109**, 167207 (2012).

[26] S. Raymond, K. Kaneko, A. Hiess, P. Steffens, and G. Lapertot, Evidence for three fluctuation channels in the spin resonance of the unconventional superconductor CeCoIn₅, Phys. Rev. Lett. **109**, 237210 (2012).

[27] J. Panarin, S. Raymond, G. Lapertot, and J. Flouquet, Evolution of the spin resonane in CeCoIn₅ under magnetic field, J. Phys. Soc. Jpn. **78**, 113706 (2009).

[28] V. S. Zapf, E. J. Freeman, E. D. Bauer, J. Petricka, C. Sirvent, N. A. Frederick, R. P. Dickey, and M. B. Maple, Coexistence of superconductivity and antiferromagnetism in CeRh$_{1-x}$Co$_x$In₅, Phys. Rev. B **65**, 014506 (2001).

[29] J. Paglione, P.-C. Ho, M. B. Maple, M. A. Tanatar, L. Taillefer, Y. Lee, and C. Petrovic, Ambient-pressure bulk superconductivity deep in the magnetic state of CeRhIn₅, Phys. Rev. B **77**, 100505(R) (2008).

[30] G. F. Chen, K. Matsubayashi, S. Ban, K. Deguchi, and N. K. Sato, Competitive coexistence of superconductivity with antiferromagnetism in CeRhIn₅, Phys. Rev. Lett. **97**, 017005 (2006).

[31] T. Park, M. J. Graf, L. Boulaevskii, J. L. Sarrao, and J. D. Thompson, Electronic duality in strongly correlated matter, Proc. Natl. Acad. Sci. USA **105**, 6825 (2008).

[32] S. Raymond, E. Ressouche, G. Knebel, D. Aoki, and J. Flouquet, Magnetic structure of CeRhIn$_5$ under magnetic field, J. Phys.: Condens. Matter **19**, 242204 (2007).

[33] C. Stock, J. A. Rodriguez-Rivera, K. Schmalzl, E. E. Rodriguez, A. Stunault, and C. Petrovic, Single to multiquasiparticle excitations in the itinerant helical magnet CeRhIn$_5$, Phys. Rev. Lett. **114**, 247005 (2015).

[34] J. A. Rodriguez, D. M. Adler, P. C. Brand, C. Broholm, J. C. Cook, C. Brocker, R. Hammond, Z. Huang, P. Hundertmakr, J. W. Lynn, N. C. Maliszewskyj, J. Moyer, J. Orndorff, D. Pierce, T. D. Pike, G. Scharfstein, S. A. Smee, and R. Vilaseca, MACS—a new high intensity cold neutron spectrometer at NIST, Meas. Sci. Technol. **19**, 034023 (2008).

[35] P. Das, S.-Z. Lin, N. J. Ghimire, K. Huang, F. Ronning, E. D. Bauer, J. D. Thompson, C. D. Batista, G. Ehlers, and M. Janoschek, Magnitude of the magnetic exchange interaction in the heavy-fermion antiferromagnet CeRhIn$_5$, Phys. Rev. Lett. **113**, 246403 (2014).

[36] D. M. Fobes, S. Zhang, S. Z. Lin, P. Das, N. J. Ghimire, E. D. Bauer, J. D. Thompson, L. W. Harriger, G. Ehlers, A. Podlesnyak, R. I. Bewley, A. Sazonov, V. Hutanu, F. Ronning, C. D. Batista, and M. Janoschek, Tunable emergent heterostructures in a prototypical correlated metal, Nat. Phys. **14**, 456 (2018).

[37] P. M. Sarte, M. Songvilay, E. Pachoud, R. A. Ewings, C. D. Frost, D. Prabhakaran, K. H. Hong, A. J. Browne, Z. Yamani, J. P. Attfield, E. E. Rodriguez, S. D. Wilson, and C. Stock, Spin-orbit excitons in CoO, Phys. Rev. B **100**, 075143 (2019).

[38] P. M. Sarte, R. A. Cowley, E. E. Rodriguez, E. Pachoud, D. Le, V. García-Sakai, J. W. Taylor, C. D. Frost, D. Prabhakaran, C. MacEwen, A. Kitada, A. J. Browne, M. Songvilay, Z. Yamani, W. J. L. Buyers, J. P. Attfield, and C. Stock, Disentangling orbital and spin exchange interactions for Co^{2+} on a rocksalt lattice, Phys. Rev. B **98**, 024415 (2018).

[39] L. Chen, H. Hu, M. G. Vergniory, J. Cano, and Q. Si, Dirac zeros in an orbital electrive Mott phase: Green's function berry curvature and flux quantization, arXiv:2401.12156

[40] R. Shiina, H. Shiba, P. Thalmeier, A. Takahashi, and O. Sakai, Dynamics of multipoles and neutron scattering spectra in quadrupolar ordering phase of CeB$_6$, J. Phys. Soc. Jpn. **72**, 1216 (2003).

[41] Y. Hasegawa and M. Matsumoto, Magnetic excitation in interacting spin trimer systems investigated by extended spin-wave theory, J. Phys. Soc. Jpn. **81**, 094712 (2012).

[42] R. A. Muniz, Y. Kato, and C. D. Batista, Generalized spin-wave theory: application to the bilinear-biquadratic model, Prog. Theor. Exp. Phys. **2014**, 83I01 (2014).

[43] K. Tomiyasu and S. Itoh, Magnetic excitations in CoO, J. Phys. Soc. Jpn. **75**, 084708 (2006).

[44] K. Yosida, *Theory of Magnetism* (Springer, Berlin, 1991).

[45] L. Allen and J. H. Eberly, *Optical Resonance and Two-Level Atoms* (Dover Publications, New York, 1987).

[46] R. A. Cowley, G. Shirane, R. J. Birgeneau, and H. J. Guggenheim, Spin fluctuations in random magnetic-nonmagnetic two-dimensional antiferromagnets. I. Dynamics, Phys. Rev. B **15**, 4292 (1977).

[47] T. Huberman, R. Coldea, R. A. Cowley, D. A. Tennant, R. L. Leheny, R. J. Christianson, and C. D. Frost, Two-magnon excitations observed by neutron scattering in the two-dimensional spin-$\frac{5}{2}$ Heisenberg antiferromagnet Rb$_2$MnF$_4$, Phys. Rev. B **72**, 014413 (2005).

[48] P. J. W. Moll, T. Helm, S. S. Zhang, C. D. Batista, N. Harrison, R. D. McDonald, L. E. Winter, B. J. Ramshaw, M. K. Chan, F. F. Balakirev, B. Batlogg, E. D. Bauer, and F. Ronning, Emergent magnetic anisotropy in the cubic heavy-fermion metal CeIn$_3$, npj Quantum Mater. **2**, 46 (2017).

[49] P. M. Sarte, C. Stock, B. R. Ortiz, K. H. Hong, and S. D. Wilson, Van Vleck excitons in Ca$_2$RuO$_4$, Phys. Rev. B **102**, 245119 (2020).

[50] W. J. L. Buyers, T. M. Holden, and A. Perreault, Temperature dependence of magnetic excitations in singlet-ground-state systems. II Excited-state spin waves near the curie temperature in Pr$_3$Tl, Phys. Rev. B **11**, 266 (1975).

[51] U. Walter, Treating crystal field parameters in lower than cubic symmetries, J. Phys. Chem. Solids **45**, 401 (1984).

[52] M. T. Hutchings, Point-charge calculations of energy levels of magnetic ions in crystalline electric fields, Solid State Phys. **16**, 227 (1964).

[53] A. D. Christianson, J. M. Lawrence, P. G. Pagliuso, N. O. Moreno, J. L. Sarrao, J. D. Thompson, P. S. Riseborough, S. Kern, E. A. Goremychkin, and A. H. Lacerda, Neutron scattering study of crystal fields in CeRhIn$_5$, Phys. Rev. B **66**, 193102 (2002).

[54] T. Willers, Z. Hu, N. Hollmann, P. O. Korner, J. Gegner, T. Burnus, H. Fujiwara, A. Tanaka, D. Schmitz, H. H. Hsieh, H. J. Lin, C. T. Chen, E. D. Bauer, J. L. Sarrao, E. Goremychkin, M. Koza, L. H. Tjeng, and A. Severing, Crystal-field and Kondo-scale investigations of CeMIn5 (M = Co, Ir, and Rh): A combined x-ray absorption and inelastic neutron scattering study, Phys. Rev. B **81**, 195114 (2010).

[55] M. Sundermann, A. Amorese, F. Strigari, B. Leedahl, L. H. Tjeng, M. W. Haverkort, H. Gretarsson, H. Yavaş, M. M. Sala, E. D. Bauer, P. F. S. Rosa, J. D. Thompson, and A. Severing, Orientation of the ground-state orbital in CeCoIn$_5$ and CeRhIn$_5$, Phys. Rev. B **99**, 235143 (2019).

[56] H. Lane, M. Songvilay, R. A. Ewings, and C. Stock, Excitonic transverse and amplitude fluctuations in noncollinear and charge-ordered RbFe^{2+}Fe^{3+}F$_6$, Phys. Rev. B **106**, 054431 (2022).

[57] E. Chan, H. Lane, J. Pásztorová, M. Songvilay, R. D. Johnson, R. Downie, J.-W. G. Bos, J. A. Rodriguez-Rivera, S.-W. Cheong, R. A. Ewings, N. Qureshi, and C. Stock, Neutron scattering sum rules, symmetric exchanges, and helicoidal magnetism in MnSb$_2$O$_6$, Phys. Rev. B **107**, 144420 (2023).

[58] H. Lane, P. M. Sarte, K. Guratinder, A. M. Arevalo-Lopez, R. S. Perry, E. C. Hunter, T. Weber, B. Roessli, A. Stunault, Y. Su, R. A. Ewings, S. D. Wilson, P. Böni, J. P. Attfield, and C. Stock, Spin-orbital correlations from complex orbital order in MgV$_2$O$_4$, Phys. Rev. Res. **5**, 043146 (2023).

[59] S. X. M. Riberolles, T. J. Slade, R. L. Dally, P. M. Sarte, B. Li, T. Han, H. Lane, C. Stock, H. Bhandari, N. J. Gimire, D. L. Abernathy, P. C. Canfield, J. W. Lynn, B. G. Ueland, and R. J. McQueeney, Orbital character of the

spin-reorientation transition in $TbMn_6Sn_6$, Nat. Commun. **14**, 2658 (2023).

[60] Z.-Y. Dong, W. Wang, and J.-X. Li, SU(n) spin-wave theory: Application to spin-orbital Mott insulators, Phys. Rev. B **97**, 205106 (2018).

[61] A. Joshi, M. Ma, F. Mila, D. N. Shi, and F. C. Zhang, Elementary excitations in magnetically ordered systems with orbital degeneracy, Phys. Rev. B **60**, 6584 (1999).

[62] Y. Q. Li, M. Ma, D. N. Shi, and F. C. Zhang, SU(4) theory for spin systems with orbital degeneracy, Phys. Rev. Lett. **81**, 3527 (1998).

[63] A. M. Perelomov, Coherent states for arbitrary Lie group, Commun. Math. Phys. **26**, 222 (1972).

[64] R. Gilmore, Geometry of symmetrized states, Ann. Phys. **74**, 391 (1972).

[65] D. J. Rowe, Boson and rotor expansions of lie algebras in vector coherent state theory, Int. J. Mod. Phys. E **02**, 119 (1993).

[66] D. J. Rowe, Vector coherent state theory: A powerful tool for solving algebraic problems in physics, in *Symmetries in Nuclear Structure*, edited by A Vitturi and R. F. Casten (World Scientific, Singapore, 2004), pp. 32–41.

[67] H. Zhang and C. D. Batista, Classical spin dynamics based on SU(N) coherent states, Phys. Rev. B **104**, 104409 (2021).

[68] D. Dahlbom, H. Zhang, Z. Laraib, D. M. Pajerowski, K. Barros, and C. Batista, Renormalized classical theory of quantum magnets, arXiv:2304.03874.

[69] D. Dahlbom, F. T. Brooks, M. S. Wilson, S. Chi, A. I. Kolesnikov, M. B. Stone, H. Cao, Y.-W. Li, K. Barros, M. Mourigal, C. D. Batista, and X. Bai, Quantum-to-classical crossover in generalized spin systems: Temperature-dependent spin dynamics of FeI_2, Phys. Rev. B **109**, 014427 (2024).

[70] W. Bao, P. G. Pagliuso, J. L. Sarrao, J. D. Thompson, Z. Fisk, J. W. Lynn, and R. W. Erwin, Incommensurate magnetic structure of $CeRhIn_5$, Phys. Rev. B **62**, R14621 (2000).

[71] A. D. Christianson, A. H. Lacerda, M. F. Hundley, P. G. Pagliuso, and J. L. Sarrao, Magnetotransport of $CeRhIn_5$, Phys. Rev. B **66**, 054410 (2002).

[72] A. Benoit, J. X. Boucherle, P. Convert, J. Flouquet, J. Palleau, and J. Schweizer, Magnetic-structure of the compound $CeIn_3$, Solid State Commun. **34**, 293 (1980).

[73] J. M. Lawrence and S. M. Shapiro, Magnetic ordering in the presence of fast spin fluctuations: A neutron scattering study of $CeIn_3$, Phys. Rev. B **22**, 4379 (1980).

[74] W. Bao, P. G. Pagliuso, J. L. Sarrao, J. D. Thompson, Z. Fisk, and J. W. Lynn, Magnetic structure of heavy-fermion Ce_2RhIn_8, Phys. Rev. B **64**, 020401(R) (2001).

[75] F. Ronning, T. Helm, K. R. Shirer, M. D. Bachmann, L. Balicas, M. K. Chan, B. J. Ramshaw, R. D. McDonald, F. F. Balakirev, M. Jaime, E. D. Bauer, and P. J. W. Moll, Electronic in-plan symmetry breaking at field-tuned quantum criticality in $CeRhIn_5$, Nature (London) **548**, 313 (2017).

[76] T. Willers, F. Strigari, Z. Hu, and A. Severing, Correlation between ground state and orbital anisotropy in heavy fermion materials, Proc. Natl. Acad. Sci. USA **112**, 2384 (2015).

[77] J. G. Rau, S. Petit, and M. J. P. Gingras, Order by virtual crystal field fluctuations in pyrochlore XY antiferromagnets, Phys. Rev. B **93**, 184408 (2016).

[78] C. Stock, J. A. Rodriguez-Rivera, K. Schmalzl, F. Demmel, D. K. Singh, F. Ronning, J. D. Thompson, and E. D. Bauer, From ising resonant fluctuations to static uniaxial order in antiferromagnetic and weakly superconducting $CeCo(In_{1-x}Hg_x)_5$(x = 0.01), Phys. Rev. Lett. **121**, 037003 (2018).

[79] W. Bao, Y. C. Gasparovic, J. W. Lynn, F. Ronning, E. D. Bauer, J. D. Thompson, and Z. Fisk, Commensurate magnetic structure of $CeRhIn_{4.85}Hg_{0.15}$, Phys. Rev. B **79**, 092415 (2009).

[80] M. Nicklas, O. Stockert, T. Park, K. Habicht, K. Kiefer, L. D. Pham, J. D. Thompson, Z. Fisk, and F. Steglich, Magnetic structure of Cd-doped $CeCoIn_5$, Phys. Rev. B **76**, 052401 (2007).

[81] K. Gofryk, F. Ronning, J.-X. Zhu, M. N. Ou, P. H. Tobash, S. S. Stoyko, X. Lu, A. Mar, T. Park, E. D. Bauer, J. D. Thompson, and Z. Fisk, Electronic tuning and uniform superconductivity in $CeCoIn_5$, Phys. Rev. Lett. **109**, 186402 (2012).

[82] Y. Song, J. V. Dyke, I. K. Lum, B. D. While, S. Jang, D. Yazici, L. Shu, A. Schneidewind, P. Cermak, Y. Qiu, M. B. Maple, D. K. Morr, and P. Dai, Robust upward dispersion of the neutron spin resonance in the heavy fermion superconductor $Ce_{1-x}Yb_xCoIn_5$, Nat. Commun. **7**, 12774 (2016).

[83] Y. Song, W. Wang, J. S. V. Dyke, N. Pouse, S. Ran, D. Yazici, A. Schneidewind, P. Cermak, Y. Qiu, M. B. Maple, D. K. Morr, and P. Dai, Nature of the spin resonance mode in $CeCoIn_5$, Commun. Phys. **3**, 98 (2020).

[84] A. V. Chubukov and L. P. Gor'kov, Spin resonance in three-dimensional superconductors: The case of $CeCoIn_5$, Phys. Rev. Lett. **101**, 147004 (2008).

[85] M. Kenzelmann, Th. Strassle, C. Niedermayer, M. Sigrist, B. Padmanabhan, M. Zolliker, A. D. Bianchi, R. Movshovich, E. D. Bauer, J. L. Sarrao, and J. D. Thompson, Coupled superconducting and magnetic order in $CeCoIn_5$, Science **321**, 1652 (2008).

[86] M. Kenzelmann, S. Gerber, N. Egetenmeyer, J. L. Gavilano, Th. Strässle, A. D. Bianchi, E. Ressouche, R. Movshovich, E. D. Bauer, J. L. Sarrao, and J. D. Thompson, Evidence for a magnetically driven superconducting q phase of $CeCoIn_5$, Phys. Rev. Lett. **104**, 127001 (2010).

[87] E. Blackburn, P. Das, M. R. Eskildsen, E. M. Forgan, M. Laver, C. Niedermayer, C. Petrovic, and J. S. White, Exploring the fragile antiferromagnetic superconducting phase in $CeCoIn_5$, Phys. Rev. Lett. **105**, 187001 (2010).

[88] G. Koutroulakis, M. D. Stewart, V. F. Mitrović, M. Horvatić, C. Berthier, G. Lapertot, and J. Flouquet, Field evolution of coexisting superconducting and magnetic orders in $CeCoIn_5$, Phys. Rev. Lett. **104**, 087001 (2010).

[89] D. N. Zubarev, Double-time Green functions in statistical physics, Sov. Phys. Usp. **3**, 320 (1960).

[90] S. Toth and B. Lake, Linear spin wave theory for single-q incommensurate magnetic structure, J. Phys.: Condens. Matter **27**, 166002 (2015).

[91] H. Lane, E. E. Rodriguez, H. C. Walker, Ch. Niedermayer, U. Stuhr, R. I. Bewley, D. J. Voneshen, M. A. Green, J. A. Rodriguez-Rivera, P. Fouquet, S.-W. Cheong, J. P. Attfield, R. A. Ewings, and C. Stock, Metastable antiphase boundary ordering in $CaFe_2O_4$, Phys. Rev. B **104**, 104404 (2021).

[92] J. Jensen and A. R. Mackintosh, *Rare Earth Magnetism: Structures and Excitations* (Clarendon Press, Oxford, 1991).